Polymer Chemistry

PAPER

Check for updates

A new amorphous dithienocyclopentapyrene-benzothiadiazole (PyDT-BT) polymer with high-mobility and strong red light emission

Tianrui Zhang,[a,b] Honglei Li,[a,b] Jichao Jiang,[a,b] Jidong Zhang,[a,b] Hongkun Tian [ID] *[a,b] and Lixiang Wang [ID] *[a,b]

Due to the contradictory molecular design principles required to achieve both high mobility and strong luminescence, the development of polymer semiconductors that simultaneously possess these characteristics remains a significant challenge. To address this issue, the development of structurally innovative conjugated polymers is highly desired. Herein, two dithienocyclopentapyrene (**PyDT**) donor units with either centro- or axial-symmetry were designed and synthesized, and subsequently copolymerized with a benzothiadiazole (**BT**) acceptor to afford **cs-PyDT-BT** and **as-PyDT-BT**. The resulting polymers exhibit pronounced position- and molecular-weight-dependent characteristics. Specifically, **cs-PyDT-BT** displays low crystallinity and a nearly amorphous microstructure, yet achieves higher charge-carrier mobility and intense red emission (∼670 nm) relative to its counterpart **as-PyDT-BT**, which shows higher crystallinity, lower mobility, and a red-shifted emission (∼690 nm). Furthermore, the influence of molecular weight was systematically investigated for **cs-PyDT-BT**. As the molecular weight increased, the film-state photoluminescence quantum yield (PLQY) gradually decreased, with the maximum value reaching 22%, while the highest mobility of 1 cm^2 V^{-1} s^{-1} was obtained at a medium M_n of approximately 100 kDa. This molecular design strategy provides new insights for developing next-generation conjugated polymers that combine strong luminescence with high mobility, thereby advancing multifunctional integrated polymeric materials.

Introduction

Conjugated polymers have emerged as crucial materials for optoelectronic devices due to their advantages of solution processability, low-cost fabrication, and tunable molecular structures for large-area electronic applications, including organic light-emitting diodes (OLEDs), organic field-effect transistors (OFETs), and so on.[1–6] These devices typically employ multi-layer architectures in which each layer exhibits its own specifically optimized function, such as high photoluminescence quantum yield (PLQY) or high charge-carrier mobility (μ).[7–9] Over the past decades, there has been significant attention to develop conjugated polymers that simultaneously combine high PLQY with high mobility, in order to develop novel devices integrating OLEDs and OFETs. For example, these could enable high-performance single-structured OLEDs and electrically-driven polymer lasers.[10–13] However, there is an inherent trade-off between the two desirable properties. The conjugated polymer materials demonstrating high charge-carrier mobility usually exhibit strong π–π stacking and good electronic coupling to ensure efficient intermolecular charge transport.[14–18] At the same time, strong π–π stacking causes fluorescence quenching due to the formation of exciplexes/excimers, charge transfer states, and the suppression of radiative recombination pathways by H-aggregate formation.[19–24] For instance, although classical diketopyrrolopyrrole (DPP)-based conjugated polymers can achieve $\mu > 1$ cm^2 V^{-1} s^{-1}, they typically show low or unreported PLQY values.[25,26] Conversely, commercially available fluorescent polymers such as poly(9,9-dioctylfluorene-*alt*-benzothiadiazole) (**F8-BT**, PLQY ≈ 50%)[25] exhibit relatively poor charge-transport performance ($\mu < 10^{-2}$ cm^2 V^{-1} s^{-1}). Therefore, designing multifunctional conjugated polymers that simultaneously combine excellent luminescent and charge-transport properties remains a significant challenge.

In past decades, significant progress has been made in developing conjugated polymers with both high charge-carrier mobility and high PLQY through rational molecular design strategies.[26–31] Among these materials, one family of conjugated polymers that has attracted particular attention is donor-*alt*-acceptor (D–A) polymers with a nearly amorphous microstructure, a low degree of energetic disorder and a special

[a]State Key Laboratory of Polymer Science and Technology, Changchun Institute of Applied Chemistry, Chinese Academy of Sciences, Changchun 130022, China. E-mail: hktian@ciac.ac.cn, lixiang@ciac.ac.cn
[b]School of Applied Chemistry and Engineering, University of Science and Technology of China, Hefei, 230026, China

charge transporting mechanism, due to an exceptionally rigid and planar backbone conformation. This unique polymer chain aggregation behaviour may provide a promising opportunity to address aforementioned trade-off. A representative polymer is indacenodithiophene-*alt*-benzothiadiazole (**IDT-BT**), exhibiting high mobility exceeding 1 cm^2 V^{-1} s^{-1} and low PLQY of 1.7% in the films.[29,32] In 2019, Sirringhaus *et al.* observed a notable influence of the side chain substitution on the nonradiative recombination dynamics of **IDT-BT** polymers.[29] The polymer M_1 with the bulkier side chains (hexadecylbenzyl) gave rise to a smaller nonradiative recombination rate than the polymer with hexadecyl chains (M_0). Although the mobility of M_1 has somewhat decreased to about 0.5 cm^2 V^{-1} s^{-1}, the film showed high PLQY of 18%, which was enhanced by an order of magnitude compared to M_0. During the same period, they further revealed that introducing much more close-crossing points into polymer aggregates, the luminescence and charge transfer properties can be simultaneously improved in such nearly amorphous polymers. By inserting benzene rings into the **IDT** backbone to extend conjugation and then increase the inter-chain interaction at close-crossing points, polymer **TIF-BT** showed simultaneously increased mobility (2.4 cm^2 V^{-1} s^{-1}) and enhanced orange-red fluorescence PLQY (~15%).[30] Recently, Chen *et al.* further extended seven ring of **TIF** to nine ring of **TTIF** and constructed polymer **TTIF-BT**, which exhibited μ of 1.1 cm^2 V^{-1} s^{-1} and PLQY of 7.6%.[31] Thus, by rational structural design, the development of new near-amorphous conjugated polymers exhibiting strong fluorescence emission and high charge transport property has become critical for further progress in this field of research.

Due to high fluorescence, efficient excimer emission, electron-rich character, polycyclic conjugation and synthetic versatility, pyrene has been widely used to construct a variety of organic semiconducting materials. A few of the pyrene-based derivatives have been reported to exhibit both strong luminescence and high charge transport capability, suggesting that the unit of pyrene would be a promising building block to construct multi-functional organic semiconductors.[33–36] Herein, two dithienocyclopentapyrene (**PyDT**) donors with different symmetries were designed and synthesized, then copolymerized with the **BT** acceptor to yield two kinds of D–A polymers **cs-PyDT-BT** and **as-PyDT-BT**. The designed pyrene-based polymers are strongly position-dependent. The centrosymmetric polymer **cs-PyDT-BT** exhibits low crystallinity and a nearly amorphous microstructure, together with higher mobility and strong fluorescence emission (~670 nm), compared to its axial-symmetric counterpart **as-PyDT-BT**, which displays relatively higher crystallinity and red-shifted emission (~690 nm). Furthermore, the influence of molecular weight on the luminescence and charge-transport properties of **cs-PyDT-BT** was investigated. It was found that with increasing molecular weight, the PLQY gradually decreased, with the highest value reaching 22%, while the maximum mobility increased to 1 cm^2 V^{-1} s^{-1} at a medium number-average molecular weight (M_n) of about 100 kDa. This molecular design strategy offers a

promising pathway toward multifunctional polymer semiconducting materials with potential applications in next-generation organic optoelectronic devices.

Results and discussion

Polymer synthesis

The synthetic routes to the **PyDT-BT** polymers are outlined in Scheme 1. At present, brominated monomer **6a** or **6b** can be obtained by 4-step reactions. Compound **3** was prepared *via* a Suzuki cross-coupling reaction between commercial compounds **1** and **2** in a yield of 70%. Then, treatment of compound **3** with an excess amount of hexadecyl magnesium bromide afforded an alcohol intermediate **4** in a yield of 36%. The synthesis can be scaled up to 10-gram quantities. Since the 1-, 3-, 6- and 8-postion of pyrene have similar reactivity, the ring-closure reaction of **4** in the presence of Amberlyst 15 (H) affords two ladder-type cores **5a** and **5b**, which can be separated by column chromatography in yields of 45% and 39%, respectively.[37] Compared to trifluoroacetic acid or *p*-toluenesulfonic acid, Amberlyst 15 (H) was found to be a more effective reagent to provide the desired products in high yields. To avoid the reaction of NBS with H atoms on the pyrene core, **5a** and **5b** underwent modified bromination reaction with multiple additions in dilute solution at −20 °C. Pure yellow solids **6a** and **6b** were obtained through recrystallization, respectively. The structures of the above compounds were verified by NMR spectroscopy and matrix-assisted laser desorption ionization time-of-flight mass spectrometry (MALDI-TOF MS).

Buchwald-G3-XPhos was chosen as the polymerization precatalyst since it enables rapid reaction to avoid deboronation of the boronate ester over time, and can produce high molecular weight polymers.[38] By controlling the feed ratio of the donor (**6a**) to acceptor (4,7-bis(4,4,5,5-tetramethyl-1,3,2-dioxaborolan-2-yl)benzo[*c*][1,2,5]thiadiazole) (**BT-Bpin**), three **cs-**
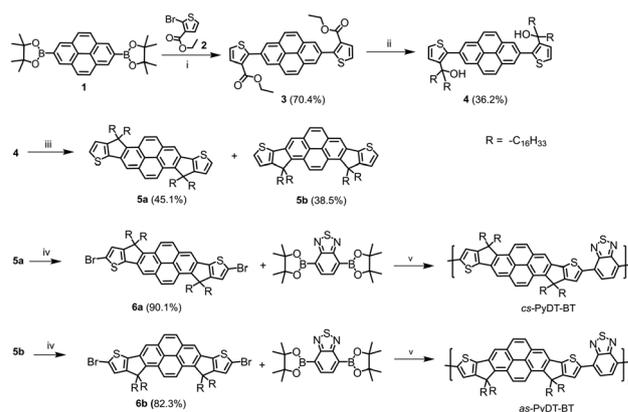
Scheme 1 Synthetic routes of the polymer **cs-PyDT-BT** and **as-PyDT-BT**. Regents and conditions: (i) Pd(PPh₃)₄, K₂CO₃, toluene/water, 110 °C; (ii) C₁₆H₃₃MgBr, THF, reflux; (iii) Amberlyst 15 (H), toluene, 110 °C; (iv) NBS, CHCl₃, −20 °C; (v) Buchwald-G3-XPhos, K₂CO₃, toluene/water, 90 °C.

PyDT-BT polymers were prepared with number-average molecular weights (M_n) and polydispersity indices (PDI) of 28 kDa and 1.73 (**cs-PyDT-BT-L**), 98 kDa and 2.51 (**cs-PyDT-BT-M**) and 171 kDa and 3.58 (**cs-PyDT-BT-H**), respectively (Fig. S1). Additionally, polymer **as-PyDT-BT** with M_n of 73.2 kDa and PDI of 2.46 was also synthesized. The polymerization details and the results of gel permeation chromatography (GPC) measurements are provided in SI. As shown in Fig. S2a, thermogravimetric analysis (TGA) results indicate that all polymers exhibit excellent thermal stability, with 5% decomposition temperatures exceeding 350 °C. Differential scanning calorimetry (DSC) measurements (Fig. S2b) reveal no significant endothermic or exothermic peaks for any of the polymers.

Photophysical and electrochemical properties

The intrinsic optical properties of these polymers were investigated through the UV-Vis absorption and photoluminescence spectra (PL) measured in solution and thin-film states. The corresponding data were summarized in Table 1. Firstly, the effects of molecular weight of **cs-PyDT-BT** on spectral behaviours were studied. As shown in Fig. S3, no significant differences can be observed. Similar behaviours with respect to molecular weight in a large range of M_n was also found in polymer **IDT-BT**.[39] Therefore, **cs-PyDT-BT-M** and **as-PyDT-BT** with comparable M_n were selected for comparison. As shown in Fig. 1a, both **cs-PyDT-BT-M** and **as-PyDT-BT** exhibited characteristic D–A polymer absorption features. The absorption band in the 450–700 nm can be attributed to intramolecular charge transfer (ICT) transitions between **PyDT** and **BT** units with distinct 0–0 and 0–1 absorption bands. The absorption band in the 300–450 nm range corresponds to π–π* transitions, in which notable strong absorption peaks from the **PyDT** subunits were observed in the range of 300–380 nm, as shown in Fig. S4. In solution, the **cs-PyDT-BT-M** showed a 0–0 absorption peak at 607 nm, while the absorption peak of **as-PyDT-BT** red-shifted by 35 nm to 642 nm. Upon going from solution to the film state, both polymers demonstrated similar absorption profiles with varying degrees of red-shift, i.e. 13 nm for **cs-PyDT-BT-M** (620 nm) and 6 nm for **as-PyDT-BT** (648 nm), respectively. These results indicate the **as-PyDT-BT** has better conjugation than **cs-PyDT-BT-M** since it has isomerized backbone. Moreover, **cs-PyDT-BT-M** exhibited a significantly lower I^{0-0}/I^{0-1} ratio and broader absorption spectra, indicating
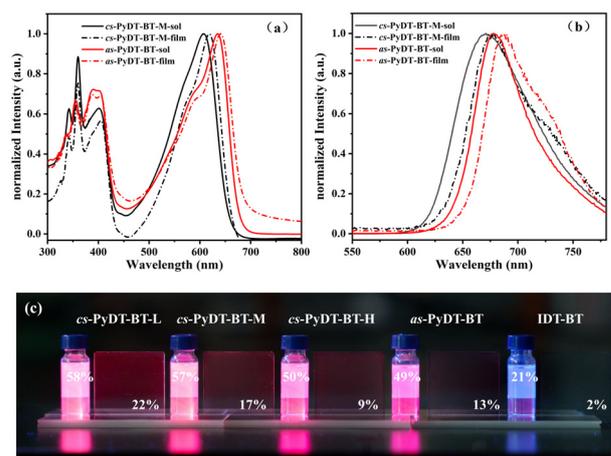

Fig. 1 (a) Normalized UV-vis absorption and (b) steady photoluminescence spectra of **cs-PyDT-BT-M** (balck) and **as-PyDT-BT** (red) in dilute solution (10^{-5} M, solid lines) and thin film (dashed lines). (c) Photographs of the emission characteristics of dilute solutions (10^{-5} M) and spin-coated films from **PyDT-BTs** and **IDT-BT** as reference under 365 nm UV irradiation. The numbers are the PLQY values.

weaker aggregation characteristics.[40] The optical bandgaps (E_g) also calculated from the onset of thin-film absorption spectra are about 2.1 eV and 2.0 eV for **cs-PyDT-BT-M** and **as-PyDT-BT**.

As illustrated in Fig. 1b, both kinds of polymers exhibit red-light emission in their steady-state photoluminescence spectra. The **cs-PyDT-BT-M** showed a maximum emission at 667 nm in solution and 670 nm in the thin-film state, while the peaks of **as-PyDT-BT** are located at 678 and 688 nm, respectively. The PLQY of all polymers was measured using an integrating sphere method and the data are summarized in Table 1. With increasing molecular weight of **cs-PyDT-BTs**, the PLQY both in solution and film state gradually decreased. Among them, **cs-PyDT-BT-L** showed the highest values of 58% in solution and 22% in the solid state. **cs-PyDT-BT-M** and **cs-PyDT-BT-H** exhibited PLQYs of 57% and 50% in solution and 17% and 9% in the film state, respectively. In contrast, **as-PyDT-BT** exhibited relatively lower PLQY of 49% in solution and 13% in the solid state than **cs-PyDT-BT-M**.

As shown in Fig. S5, the behavior of aggregation-caused quenching (ACQ) can be clearly observed for these polymers. Moreover, as M_n of the **cs-PyDT-BTs** increases, the PL intensity

Table 1 Summary of the properties of these polymers

Polymer	M_n/PDI [kDa/—]	$\lambda_{abs}^{sol\ a}$ [nm]	$\lambda_{abs}^{film\ b}$ [nm]	$\lambda_{emi}^{sol\ c}$ [nm]	$\lambda_{emi}^{film\ d}$ [nm]	$E_g^{\ e}$ [eV]	HOMO^f [eV]	LUMO^g [eV]	PLQY^h [%]	PLQY^i [%]
cs-PyDT-BT-L	27.8/1.73	605	622	667	671	2.16	−5.55	−3.29	58%	22
cs-PyDT-BT-M	97.6/2.51	607	620	667	670	2.13	−5.53	−3.32	57%	17
cs-PyDT-BT-H	170.8/3.58	607	618	667	670	2.14	−5.55	−3.32	50%	9
as-PyDT-BT	73.2/2.46	642	648	678	688	2.01	−5.35	−3.31	49%	13

^{a} Absorption maximum in o-dichlorobenzene (o-DCB) solution (10^{-5} M). ^{b} Absorption maximum in the spin-coated film. ^{c} Emission maximum in o-DCB (10^{-5} M). ^{d} Emission maximum in the spin-coated film. ^{e} E_g determined from the onset of thin-film absorption spectra. ^{f} Calculated from oxidation onset of cyclic voltammetry (CV) curves, respectively. ^{g} Calculated from reduction onset of cyclic voltammetry (CV) curves, respectively. ^{h} PLQY in the o-xylene solution (10^{-5} M). ^{i} PLQY in the film state.

weakens more rapidly. Additionally, transient photo-luminescence spectra of **cs-PyDT-BTs** (Fig. S6) all showed two stages of exponential decay in the thin films, the former possibly originating from aggregated luminescence. With increasing M_n of the **cs-PyDT-BTs**, the lifetimes were 0.99, 0.66 and 0.49 ns, indicating enhanced ACQ tendency. Therefore, we thought these polymers could form some extent of aggregation in both solution and film. A similar situation was also observed in the red-emissive polymer meso-TBTF.[41] The decay times on the nanosecond scale indicate these polymers are fluorescent emitters.

The highest occupied molecular orbital (HOMO) and the lowest unoccupied molecular orbital (LUMO) energy levels of the polymers were estimated from the onsets of oxidation and reduction potentials measured by cyclic voltammetry (CV), as summarized in Table 1 and Fig. S7. **cs-PyDT-BTs** and **as-PyDT-BT** have similar LUMO energy levels of about −3.3 eV, while the former shows 0.2 eV lower-lying HOMO level than the latter (−5.5 vs. −5.3 eV).

Thin film morphology

To further explore the difference in microstructure, two-dimensional grazing-incidence wide-angle X-ray scattering (2D-GIWAXS) was utilized to characterize polymer chain packing behavior. The films were formed through drop-casting using o-DCB as the solvent, followed by thermal annealing at 150 °C for 30 minutes. Because of the same film preparation conditions and similar film thickness (~600 nm), the diffraction patterns of these polymer films were comparable. The corresponding 2D-GIWAXS patterns are presented in Fig. 2, along with analyses of in-plane and out-of-plane diffraction peaks shown in Fig. S8.

As shown in Fig. 2a, c and e, the **cs-PyDT-BTs** exhibit nearly amorphous packing characteristics like the classic **IDT-BT**

polymer.[29,42] The presence of (100) and (010) diffractions in the q_z (out-of-plane) direction, along with (100) and (010) signals in the q_{xy} (in-plane) direction, indicate the crystallites adopt a bimodal distribution of edge-on and face-on orientations. The π–π stacking distances of ~4.1 Å for **cs-PyDT-BTs** could be obtained from the (010) diffraction at $q_z \approx 1.53$ Å^{-1}, overlapping with the diffuse diffraction rings from alkyl chain packing. Among the three polymers with different M_n, **cs-PyDT-BT-M** exhibited the strongest out-of-plane (010) diffraction, indicating a higher extent of π-aggregation and implying this polymer could exhibit a better charge-carrier-transport capability than the other two. The diffraction signals at $q_{xy} = 0.48$ Å^{-1} can probably be assigned to the (002) diffraction along the conjugation backbone, corresponding to a d-spacing of 13.09 Å. In contrast, the **as-PyDT-BT** demonstrates significantly higher crystallinity. Along the q_z direction, (h00) diffraction peaks up to (300), corresponding to lamellar packing, were observed with a d-spacing of 20.26 Å. The relative degree of crystallinity (r-DoC) values of 1 and 0.72 for **as-PyDT-BT** and **cs-PyDT-BT-M** can be obtained, according to the relative intensity of (100) diffractions. Notably, no distinct (010) diffraction could be observed in the q_{xy} direction. Meanwhile, in the q_z direction, the diffraction arc with a d-spacing of 4.08 Å can be identified as (010). This pattern indicates the polymer chains adopt a mixed orientation in a predominantly edge-on motif. The in-plane diffraction signals at $q_{xy} = 0.53$, 1.06 and 1.59 Å^{-1} are assigned to (002), (004) and (006) diffractions, corresponding to d-spacings of 11.86, 5.93 and 3.95 Å, implying that **as-PyDT-BT** has a more regular backbone. As listed in Table 2, their coherence lengths (CLs) were also calculated. It is found that **as-PyDT-BT** exhibits more ordered lamellar packing and less ordered π–π stacking than **cs-PyDT-BTs**. Moreover, in the series of **cs-PyDT-BTs** with varied molecular weights, **cs-PyDT-BT-M** showed the largest CLs of (100) and (010) diffrac-
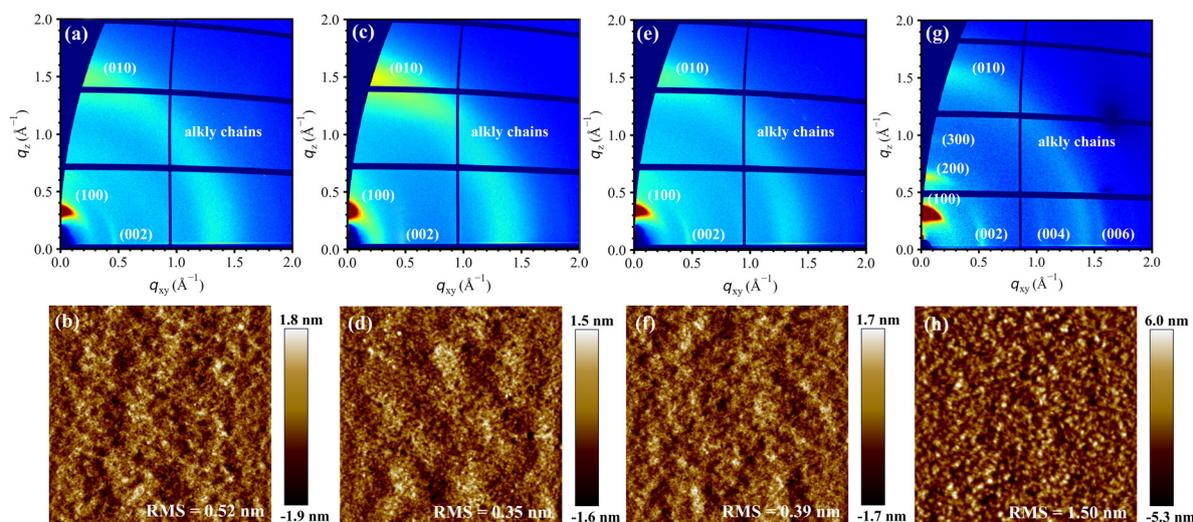

Fig. 2 2D-GIWAXS patterns and AFM height images (2 μm × 2 μm) of (a) and (b) **cs-PyDT-BT-L**, (c) and (d) **cs-PyDT-BT-M**, (e) and (f) **cs-PyDT-BT-H**, (g) and (h) **as-PyDT-BT**. The root-mean-square (RMS) surface roughness is also provided. The films of 2D-GIWAXS patterns were deposited by drop-casted and annealed at 150 °C for 30 min.

Table 2 Characteristics of the 2D-GIWAXS results of drop-casted polymer films

Polymers	d-spacing [Å]							CLs [Å]	
	(100)	(200)	(300)	(010)	(002)	(004)	(006)	(100)	(010)
cs-PyDT-BT-L	20.26	—	—	4.09	13.09	—	—	90	20
cs-PyDT-BT-M	20.26	—	—	4.10	13.09	—	—	93	22
cs-PyDT-BT-H	20.23	—	—	4.08	13.09	—	—	89	18
as-PyDT-BT	20.26	9.82	6.93	4.08	11.86	5.93	3.95	119	14

tion peaks in the q_z direction, which further indicates that this polymer can exhibit good transporting capability. Their significantly different packing behaviors will inevitably influence their transporting and optical properties.

As shown in Fig. 2 and Fig. S9, the thin film surface morphology of **cs-PyDT-BTs** and **as-PyDT-BT** was investigated by atomic force microscopy (AFM). **cs-PyDT-BTs** exhibit a uniform height image. With increasing the M_n, the root mean square (RMS) roughness exhibited downward trends with the values of 0.52 nm for **cs-PyDT-BT-L**, 0.35 nm for **cs-PyDT-BT-M** and 0.39 nm for **cs-PyDT-BT-H**, respectively. In contrast, **as-PyDT-BT** exhibits a quasi-fibrillar morphology with an RMS roughness of 1.50 nm, consistent with higher crystallinity.

Theoretical investigation of polymer properties

To better understand the aggregation behavior of these polymers, theoretical calculations based on density functional theory (DFT) were performed. As shown in Fig. 3a, the torsional potential energy surface (PES) scanning calculations between **PyDT** and adjacent **BT** units were employed to understand the relative conformations of the two units and to infer backbone torsional disorder, in comparison with **IDT-BT**. The calculations were conducted at the B3LYP/6-31G(d,p) level, with long alkyl side chains replaced by methyl groups to simplify the computations. The three polymers exhibited the similar results to the overall PES plots because they have analogous pentadiene-thiophene substructures and non-covalent

interactions. The energy minima appear at dihedral angles of 0° and 180°, corresponding to conformations A and B, suggesting the polymers have the tendency to form planar and rigid backbone structures with low torsional disorder. The large rotational energy barriers of ~6 kcal mol^{-1} indicate that both conformations are relatively stable and may coexist within the polymer chains.

For polymer **cs-PyDT-BT**, the energy difference between the two conformations is so minimal (~ 0.3 kcal mol^{-1}), yet the energy barrier is substantially high, suggesting that conformations A and B likely coexist. This phenomenon may arise from the lack of conformational selectivity during the polymerization of **cs-PyDT** monomer. In contrast, the axially symmetric **as-PyDT** monomer, with all alkyl chains oriented toward the same side, experiences greater steric hindrance effects between adjacent connecting units. This leads **as-PyDT-BT** to preferentially form alternating pattern of conformations A and B to minimize energy.

Consequently, we selected alternating conformations that better represent the behavior of actual polymers to investigate the potential impact of backbone geometries on polymer interchain packing. As shown in Fig. 3b, geometry optimization was performed on tetramers using the B3LYP/6-31G(d,p) basis set. The **as-PyDT-BT** polymer exhibited an extremely small dihedral angle of approximately 0°, demonstrating high planarity and a rigid backbone. In contrast, **cs-PyDT-BT** showed larger dihedral angles, indicating inferior planarity compared to **as-PyDT-BT**.

As mentioned previously, we used alternating conformations to compare the two polymers. For the **cs-PyDT-BT** polymer, fragments with either entirely conformation A or entirely conformation B might also exist. Theoretical simulations for both cases were also conducted, as shown in Fig. S10. Both conformations exhibited a wave-like backbone yet rigid backbone. The polymer adopting conformation A displayed excellent planarity, while the polymer adopting conformation B showed larger dihedral angles. This pattern is consistent with the angular differences observed in the alternating conformations.

Both polymers showed well-delocalized HOMO orbitals, with corresponding calculated energy levels of −4.83 eV for **cs-PyDT-BT** and −4.74 eV for **as-PyDT-BT**. The results were consistent with electrochemical CV characterization, which reveals the reliability of the DFT results. The LUMO was primarily distributed on the acceptor units, with similar calculated values of −2.73 eV for **cs-PyDT-BT** and −2.74 eV for **as-PyDT-BT**.
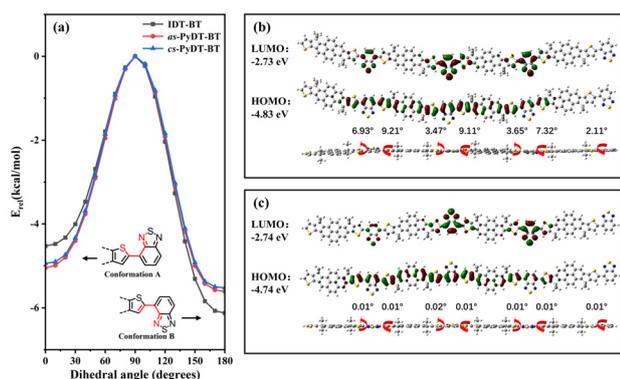

Fig. 3 (a) Calculated torsional PES of **cs-PyDT-BT**, **as-PyDT-BT** and **IDT-BT** based on DFT calculations at B3LYP/6-31G (d,p) level, the alkyl chains were replaced by methyl groups for simplicity. The optimized molecular structure and frontier molecular orbitals of (b) **cs-PyDT-BT** and (c) **as-PyDT-BT** (top, LUMO; central, HOMO; bottom, side view).

OFET and OLED devices

Top-gate/bottom-contact (TG/BC) OFET devices were fabricated to evaluate charge transport properties of these polymers. Fig. 4 displays typical transfer in saturation region and output curves of these devices and Fig. S11 displays typical transfer curves in linear region. The hole mobility (μ_h), threshold voltage (V_{th}), and on/off current ratio (I_{on}/I_{off}) were extracted from the transfer curves in the saturation regime and summarized in Table 3. For **cs-PyDT-BTs**, the average mobilities increased from 0.59 (**cs-PyDT-BT-L**) to 0.80 cm^2 V^{-1} s^{-1} (**cs-PyDT-BT-M**). However, due to decreased solubility and processability of high molecular weight polymer **cs-PyDT-BT-H**, the devices exhibited a somewhat decline in transport capability with average mobility of 0.50 cm^2 V^{-1} s^{-1}. It is clear that the mobility trend followed that of the CLs for (010) diffractions, as revealed by the 2D-GIWAXS results (Fig. S8 and Table 2). Additionally, the **cs-PyDT-BT-M** devices exhibited a maximum μ_h of 1.03 cm^2 V^{-1} s^{-1}. In contrast, **as-PyDT-BT** devices showed significantly lower transport performance, with an average μ_h of 0.002 cm^2 V^{-1} s^{-1}. Fig. S12 illustrates the typical relationship between μ_h and gate voltage (V_{GS}) in OFET devices, and shows no significant dependence of effective mobility on gate voltage. Since the polymer **as-PyDT-BT** has a higher-lying HOMO energy level than **cs-PyDT-BTs**, the devices exhibited relatively lower V_{th} values.

Based on structural characterization and transport performance, distinct packing and transport models for the two polymers were proposed. As illustrated in Fig. 5, like the classic
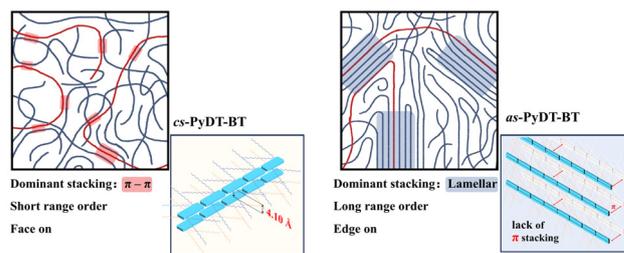

Fig. 5 Schematic illustration of the microstructure of **cs-PyDT-BT** and **as-PyDT-BT**. In **cs-PyDT-BT** with nearly amorphous microstructure, the elongated polymer chains (highlighted in red) can form continuous charge transport pathways. In this case, short-range ordering driven by $\pi-\pi$ interactions (as illustrated in the zoomed-in region) facilitates hole hopping between chains. In contrast, the semi-crystalline polymer **as-PyDT-BT** exhibits long-range ordered domains dominated by lamellar packing, yet the lack of effective $\pi-\pi$ stacking results in significantly degraded device performance.

IDT-BT polymer, **cs-PyDT-BT** forms nearly amorphous films with mixed face-on and edge-on orientation. Despite its low crystallinity and lack of long-range order, the transport performance of **cs-PyDT-BT** is primarily attributed to charge transport predominantly occurring along the conjugated polymer chains, with occasional hopping between inter-chain π-interactions.[39] In contrast, **as-PyDT-BT** forms semi-crystalline films. The lack of efficient $\pi-\pi$ interactions hinders effective charge hopping, thus impacting its transport capabilities.

Given the excellent optical performance of **cs-PyDT-BT-L**, polymer light-emitting diodes (PLEDs) were fabricated to further demonstrate its electroluminescent properties. The device structure is shown in Fig. 6: ITO (150 nm)/PEDOT:PSS/ Emitting layer (EML)/SPPO13 (55 nm)/LiF (1 nm)/Al (150 nm), where PEDOT:PSS acts as the hole transport layer and SPPO13 serves as the electron transporting and hole blocking layer. CBP was used as the host material in the EML, and the electroluminescent properties of the polymer were optimized at different doping concentrations (Fig. S13 and Table S1). The devices with a doped ratio of 6% exhibited a high brightness of 226 cd cm^{-2}, a low turn-on voltage of 4.9 V, and a maximum external quantum efficiency of 0.72%. The electroluminescence spectra overlapped with the corresponding PL spectra, with no host emission observed. In PLED devices with different doping concentrations, the EL spectral emission peaks remained nearly unchanged, further demonstrating the weak aggregation characteristics of **cs-PyDT-BT**. These results suggest that **cs-PyDT-BTs**, featuring high mobility (μ_{max} up to
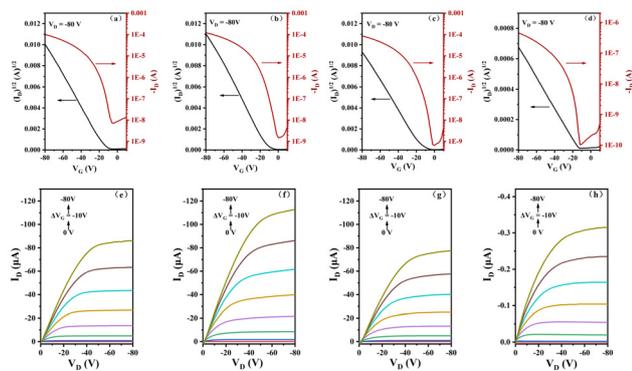

Fig. 4 The representative transfer characteristics and output characteristics of **cs-PyDT-BT-L** (a and e), **cs-PyDT-BT-M** (b and f), **cs-PyDT-BT-H** (c and g), **as-PyDT-BT** (d and h) in the TG/BC OFET devices.

Table 3 Summary of the electrical performance of **cs-PyDT-BTs** and **as-PyDT-BT**

Polymer	μ_{ave} [cm^2 V^{-1} s^{-1}]	μ_{max} [cm^2 V^{-1} s^{-1}]	V_{th} [V]	I_{on}/I_{off}	μ_{ave}^{linear} [cm^2 V^{-1} s^{-1}]
cs-PyDT-BT-L	0.59 ± 0.06	0.64	−10 to −17	10^3 to 10^5	0.48 ± 0.04
cs-PyDT-BT-M	0.80 ± 0.12	1.03	−12 to −24	10^4 to 10^5	0.53 ± 0.08
cs-PyDT-BT-H	0.50 ± 0.09	0.64	−11 to −22	10^4 to 10^5	0.49 ± 0.1
as-PyDT-BT	0.002 ± 0.0003	0.0025	−10 to −14	10^3 to 10^4	0.0016 ± 0.0005

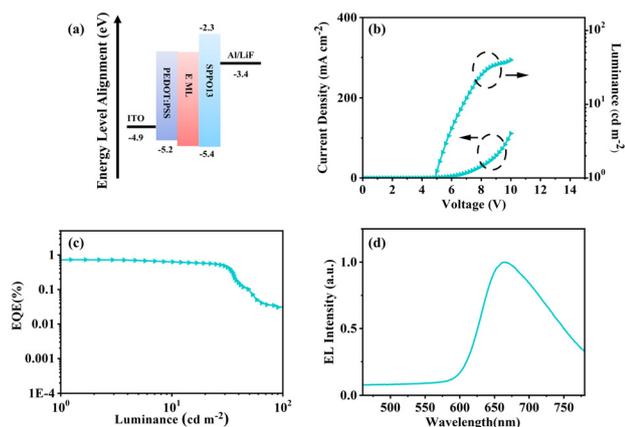All average values in OTFT are extracted from over ten devices.

Fig. 6 The energy level diagram (a), current density−voltage−luminance (*J*−*V*−*L*) characteristics (b), EQE as a function of luminance (c) and EL spectra at 100 cd m^{-2} (d) of the of **cs-PyDT-BT-L** PLEDs devices with 6% doping in CBP.

1.03 cm^2 V^{-1} s^{-1}), high PLQY (up to 22%), and red emission, exhibit performance metrics that rank among the best reported for red light-emitting polymer semiconductors (Table S2), highlighting their strong potential for further application in optoelectronic devices.

Conclusions

The novel electron-rich units-dithienocyclopentapyrene (**PyDT**) based on a promising multi-functional building block pyrene, were designed and synthesized, then two D–A **PyDT-BT** polymers (**cs-PyDT-BT** and **as-PyDT-BT**) were obtained. Notably, these two polymers are strongly position- and molecular weight-dependent. Although **cs-PyDT-BT** shows lower crystallinity with nearly amorphous aggregation characteristics, **cs-PyDT-BT** demonstrated higher charge carrier transport capability and stronger solid-state red emission compared with **as-PyDT-BT**. Remarkably, **cs-PyDT-BT-M** exhibited a hole mobility up to 1 cm^2 V^{-1} s^{-1} with a film-state PLQY of 17%—metrics that represent some of the best reported values for red light-emitting polymer semiconductors. We believe that **Py-BT** class structure and their derivative fully rigid coplanar conjugated polymer semiconductors can provide a useful platform for the fabrication of multi-functional organic opto-electronic device in the future.

Conflicts of interest

There are no conflicts to declare.

Data availability

The authors confirm that the data supporting the findings of this study are available in the supplementary information (SI). Supplementary information: instruments, experimental

details, characterization of OFET and OLED devices, TGA and DSC curves of these polymers and other theoretical investigation data. See DOI: https://doi.org/10.1039/d5py00990a.

References

1 J. H. Burroughes, D. D. C. Bradley, A. R. Brown, R. N. Marks, K. Mackay, R. H. Friend, P. L. Burns and A. B. Holmes, *Nature*, 1990, **347**, 539–541.

2 J. Ouyang, *SmartMat*, 2021, **2**, 263–285.

3 J. M. Dos Santos, D. Hall, B. Basumatary, M. Bryden, D. Chen, P. Choudhary, T. Comerford, E. Crovini, A. Danos, J. De, S. Diesing, M. Fatahi, M. Griffin, A. K. Gupta, H. Hafeez, L. Hämmerling, E. Hanover, J. Haug, T. Heil, D. Karthik, S. Kumar, O. Lee, H. Li, F. Lucas, C. F. R. Mackenzie, A. Mariko, T. Matulaitis, F. Millward, Y. Olivier, Q. Qi, I. D. W. Samuel, N. Sharma, C. Si, L. Spierling, P. Sudhakar, D. Sun, E. Tankelevičiūtė, M. Duarte Tonet, J. Wang, T. Wang, S. Wu, Y. Xu, L. Zhang and E. Zysman-Colman, The Golden Age of Thermally Activated Delayed Fluorescence Materials: Design and Exploitation, *Chem. Rev.*, 2024, **124**(24), 13736–14110.

4 A. C. Arias, J. D. MacKenzie, I. McCulloch, J. Rivnay and A. Salleo, Materials and Applications for Large Area Electronics: Solution-Based Approaches, *Chem. Rev.*, 2010, **110**(1), 3–24.

5 P. Wang, J. Yang, Y. Zhang, W. Hu and H. Dong, Near-Amorphous Conjugated Polymers: An Emerging Class of Semiconductors for Flexible Electronics, *ACS Mater. Lett.*, 2022, **4**(6), 1112–1123.

6 L. Ding, Z.-D. Yu, X.-Y. Wang, Z.-F. Yao, Y. Lu, C.-Y. Yang, J.-Y. Wang and J. Pei, Polymer Semiconductors: Synthesis, Processing, and Applications, *Chem. Rev.*, 2023, **123**(12), 7421–7497.

7 A. Nawaz, L. Merces, L. M. M. Ferro, P. Sonar and C. C. B. Bufon, Impact of Planar and Vertical Organic Field-Effect Transistors on Flexible Electronics, *Adv. Mater.*, 2023, **35**, 2204804.

8 J. Bauri, R. B. Choudhary and G. Mandal, Recent advances in efficient emissive materials-based OLED applications: a review, *J. Mater. Sci.*, 2021, **56**, 18837–18866.

9 D. Yuan, V. Sharapov, X. Liu and L. Yu, Design of High-Performance Organic Light-Emitting Transistors, *ACS Omega*, 2020, **5**, 68–74.

10 M. Muccini, A bright future for organic field-effect transistors, *Nat. Mater.*, 2006, **5**, 605–613.

11 K. Yoshida, J. Gong, A. L. Kanibolotsky, P. J. Skabara, G. A. Turnbull and I. D. W. Samuel, Electrically driven organic laser using integrated OLED pumping, *Nature*, 2023, **621**, 746–752.

12 G. Sharma, S. Kattayat, S. F. Naqvi, S. Z. Hashmi and P. A. Alvi, Role of MEH:PPV polymer in single layer OLEDs with its optoelectronic Characteristics, *Mater. Today: Proc.*, 2021, **42**, 1678–1681.

13 Z. Qin, H. Gao, H. Dong and W. Hu, Organic Light-Emitting Transistors Entering a New Development Stage, *Adv. Mater.*, 2021, **33**, 2007149.

14 Z. Liu, G. Zhang and D. Zhang, Molecular Materials That Can Both Emit Light and Conduct Charges: Strategies and Perspectives, *Chem. – Eur. J.*, 2016, **22**, 462–471.

15 A. Troisi, The speed limit for sequential charge hopping in molecular materials, *Org. Electron.*, 2011, **12**(12), 1988–1991.

16 O. V. Mikhnenko, M. Kuik, J. Lin, N. van der Kaap, T.-Q. Nguyen and P. W. M. Blom, Trap-Limited Exciton Diffusion in Organic Semiconductors, *Adv. Mater.*, 2014, **26**, 1912–1917.

17 R. C. Hilborn, Einstein coefficients, cross sections, f values, dipole moments, and all that, *Am. J. Phys.*, 1982, **50**(11), 982–986.

18 B. K. Yap, R. Xia, M. Campoy-Quiles, P. N. Stavrinou and D. D. C. Bradley, Simultaneous optimization of charge-carrier mobility and optical gain in semiconducting polymer films, *Nat. Mater.*, 2008, **7**(5), 376–380.

19 A. Sharma, M. M. Hasan and Y. Lu, Exciton dynamics in 2D organic semiconductors, *Mater. Futures*, 2022, **1**, 042001.

20 T. Horio, T. Fuji, Y.-I. Suzuki and T. Suzuki, Probing Ultrafast Internal Conversion through Conical Intersection via Time-Energy Map of Photoelectron Angular Anisotropy, *J. Am. Chem. Soc.*, 2009, **131**, 10392–10393.

21 F. Cacialli, J. S. Wilson, J. J. Michels, C. Daniel, C. Silva, R. H. Friend, N. Severin, P. Samorì, J. P. Rabe, M. J. O'Connell, P. N. Taylor and H. L. Anderson, Cyclodextrin-threaded conjugated polyrotaxanes as insulated molecular wires with reduced interstrand interactions, *Nat. Mater.*, 2002, **1**(3), 160–164.

22 M. Y. Wong, Recent Advances in Polymer Organic Light-Emitting Diodes (PLED) Using Non-conjugated Polymers as the Emitting Layer and Contrasting Them with Conjugated Counterparts, *J. Electron. Mater.*, 2017, **46**(11), 6246–6281.

23 C. Zhang, P. Chen and W. Hu, Organic Light-Emitting Transistors: Materials, Device Configurations, and Operations, *Small*, 2016, **12**(10), 1252–1294.

24 K. Liu, Y. Gu, Z. Yi and Y. Liu, Diketopyrrolopyrrole-based Conjugated Polymers as Representative Semiconductors for High-Performance Organic Thin-Film Transistors and Circuits, *Chin. J. Polym. Sci.*, 2023, **41**(5), 671–682.

25 M. Gwinner, Y. Vaynzof, K. Banger, P. Ho, R. Friend and H. Sirringhaus, Solution–Processed Zinc Oxide as High–Performance Air–Stable Electron Injector in Organic Ambipolar Light–Emitting Field–Effect Transistors, *Adv. Funct. Mater.*, 2010, **20**, 3457–3465.

26 J. Chen, M. Zhu, M. Shao, W. Shi, J. Yang, J. Kuang, C. Wang, W. Gao, C. Zhu, R. Meng, Z. Yang, Z. Shao, Z. Zhao, Y. Guo and Y. Liu, Molecular Design of Multifunctional Integrated Polymer Semiconductors with Intrinsic Stretchability, High Mobility, and Intense Luminescence, *Adv. Mater.*, 2024, **36**, 2305987.

27 J. Chen, J. Kuang, Y. Liu, J. Yang, M. Zhu, X. Wei, M. Shao, Z. Zhao, Y. Guo and Y. Liu, Regioregular Pyridal[1,2,3] Triazole–Based Polymer Semiconductors for High Mobility and Near–Infrared Light Emission Applications, *Adv. Opt. Mater.*, 2022, **10**, 2201243.

28 Y. Zhang, C. Xu, P. Wang, C. Gao, W. Li, Z. Ni, Y. Han, Y. Zhao, Y. Geng, Z. Wang, W. Hu and H. Dong, Universal Design and Efficient Synthesis for High Ambipolar Mobility Emissive Conjugated Polymers, *Angew. Chem., Int. Ed.*, 2024, **63**, e202319997.

29 T. Thomas, J. Rivett, Q. Gu, D. Harkin, J. M. Richter, A. Sadhanala, C. Yong, S. Schott, K. Broch, J. Armitage, A. Gillett, S. Menke, A. Rao, D. Credgington and H. Sirringhaus, Chain Coupling and Luminescence in High-Mobility, Low-Disorder Conjugated Polymers, *ACS Nano*, 2019, **13**, 13716–13727.

30 T. Thomas, D. Harkin, A. Gillett, V. Lemaur, M. Nikolka, A. Sadhanala, J. Richter, J. Armitage, H. Chen, I. McCulloch, S. Menke, Y. Olivier, D. Beljonne and H. Sirringhaus, Short contacts between chains enhancing luminescence quantum yields and carrier mobilities in conjugated copolymers, *Nat. Commun.*, 2019, **10**, 2614.

31 M. Wang, G. Xia, C. Yang, L. Zhang, M. Nikolka, W. Zhang, C. Cendra, W. Liu, S. Zhao, J. Zeng, C. Zou, J. Gorenflot, A. Salleo, F. Laquai, H. Sirringhaus, I. McCulloch and H. Chen, An Amorphous Donor–Acceptor Conjugated Polymer with Both High Charge Carrier Mobility and Luminescence Quantum Efficiency, *Angew. Chem., Int. Ed.*, 2025, **64**, e202421199.

32 A. Wadsworth, H. Chen, K. Thorley, C. Cendra, M. Nikolka, H. Bristow, M. Moser, A. Salleo, T. D. Anthopoulos, H. Sirringhaus and I. McCulloch, Modification of Indacenodithiophene-Based Polymers and Its Impact on Charge Carrier Mobility in Organic Thin-Film Transistors, *J. Am. Chem. Soc.*, 2020, **142**, 652–664.

33 Y. Gong, X. Zhan, Q. Li and Z. Li, Progress of pyrene-based organic semiconductor in organic field effect transistors, *Sci. China: Chem.*, 2016, **59**(12), 1623–1631.

34 K. Oniwa, H. Kikuchi, H. Shimotani, S. Ikeda, N. Asao, Y. Yamamoto, K. Tanigaki and T. Jin, 2-Positional pyrene end-capped oligothiophenes for high performance organic field effect transistors, *Chem. Commun.*, 2016, **52**, 4800.

35 H. Ju, K. Wang, J. Zhang, H. Geng, Z. Liu, G. Zhang, Y. Zhao and D. Zhang, 1,6- and 2,7-trans-β-Styryl Substituted Pyrenes Exhibiting Both Emissive and Semiconducting Properties in the Solid State, *Chem. Mater.*, 2017, **29**, 3580–3588.

36 H. Liu, Z. Xu, J. Zhang, L. Rao, Y. Ge, Z. Xia, X. Zhang, L. Jiang, Y. Yi, B. Yang and Y. Ma, Integrating Strong Luminescence and High Mobility in Organic Single Crystals of Covalent Pyrene Dimers, *Adv. Mater.*, 2025, **37**, 2419981.

37 J. Wu, Y. Chen, B. Hu, Z. Pang, Z. Lu and Y. Huang, Isomers of Dithienocyclopentapyrene–Based Non–Fullerene Electron Acceptors: Configuration Effect on Photoelectronic Properties, *Chem. – Eur. J.*, 2019, **25**, 6385–6391.

38 Y. Yamada and A. Sen, Latest Developments on Palladium- and Nickel-Catalyzed Cross-Couplings Using Aryl Chlorides: Suzuki–Miyaura and Buchwald–Hartwig Reactions, *Synthesis*, 2024, 3555–3574.

39 B. Zhao, D. Pei, Y. Jiang, Z. Wang, C. An, Y. Deng, Z. Ma, Y. Han and Y. Geng, Simultaneous Enhancement of Stretchability, Strength, and Mobility in Ultrahigh-Molecular-Weight Poly(indacenodithiophene-co-benzothiadiazole), *Macromolecules*, 2021, **54**, 9896–9905.

40 F. Spano and C. Silva, H- and J-Aggregate Behavior in Polymeric Semiconductors, *Annu. Rev. Phys. Chem.*, 2014, **65**, 477–500.

41 X. Guo, Y. Zhang, Y. Hu, J. Yang, Y. Li, Z. Ni, H. Dong and W. Hu, Molecular Weight Engineering in High-Performance Ambipolar Emissive Mesopolymers, *Angew. Chem., Int. Ed*, 2021, **60**, 14902–14908.

42 X. Zhang, H. Bronstein, A. Kronemeijer, J. Smith, Y. Kim, R. Kline, L. Richter, T. Anthopoulos, H. Sirringhaus, K. Song, M. Heeney, W. Zhang, I. McCulloch and D. DeLongchamp, Molecular origin of high field-effect mobility in an indacenodithiophene–benzothiadiazole copolymer, *Nat. Commun.*, 2013, **4**(1), 2238.